Dynamic estimation of the attentional field from visual cortical activity

Ilona M. Bloem[1,2]*, Leah Bakst[1]*, Joseph T. McGuire[1], Sam Ling[1]

[1] Department of Psychological & Brain Sciences, Boston University, Boston, USA
[2] Department of Computational Cognitive Neuroscience and Neuroimaging, Netherlands Institute for Neuroscience, Amsterdam, Netherlands & Spinoza Centre for Neuroimaging, Amsterdam, Netherlands

* These authors provided equal contribution

Correspondence should be addressed to Sam Ling (samling@bu.edu).

Abbreviated title (50-character max): Dynamical estimation of the attentional field

Number of pages: 25
Number of figures: 6
Number of words for:
    Abstract: 247
    Introduction: 649
    Discussion: 1149

The authors declare no competing financial interests.

Author contributions: Conceptualization, Methodology & Writing – Review & Editing I.M.B., L.B., J.T.M., S.L.; Investigation, Analysis, Visualization, & Writing – Original Draft, I.M.B. & L.B.; Resources & Supervision, J.T.M & S.L.; Funding Acquisition L.B., J.T.M., S.L.

Abstract

Navigating around the world, we must adaptively allocate attention to our surroundings based on anticipated future stimuli and events. This allocation of spatial attention boosts visuocortical representations at attended locations and locally enhances perception. Indeed, spatial attention has often been analogized to a "spotlight" shining on the item of relevance. Although the neural underpinnings of the locus of this attentional spotlight have been relatively well studied, less is known about the size of the spotlight: to what extent can the attentional field be broadened and narrowed in accordance with behavioral demands? In this study, we developed a paradigm for dynamically estimating the locus and spread of covert spatial attention, inferred from visuocortical activity using fMRI in humans. We measured BOLD activity in response to an annulus while participants (4 female, 4 male) used covert visual attention to determine whether more numbers or letters were present in a cued region of the annulus. Importantly, the width of the cued area was systematically varied, calling for different sizes of the attentional spotlight. The deployment of attention was associated with an increase in BOLD activity in corresponding retinotopic regions of visual areas V1—V3. By modeling the visuocortical attentional modulation, we could reliably recover the cued location, as well as a broadening of the attentional enhancement with wider attentional cues. This modeling approach offers a useful window into the dynamics of attention and spatial uncertainty.

Significance Statement

This study explores whether spatial attention can dynamically adapt by shifting and broadening the attentional field. While previous research has focused on the modulation of neural responses at attended locations, less is known about how the size of the attentional field is represented within visual cortex. Using fMRI, we developed a novel paradigm to estimate the spatial tuning of the attentional field and demonstrate that we were able to recover both the location as well as the width of the attentional field. Our findings offer new insights into the neural mechanisms underlying the deployment of spatial attention, contributing to a deeper understanding of how spatial attention supports visual perception.

Introduction

70

71   We bounce attention around all the time. Take, for instance, when we're monitoring
72   oncoming traffic while driving. It isn't sufficient to attend to the single most likely source
73   of traffic. Instead, attention adaptively broadens and narrows to cover the anticipated
74   spatial distribution of relevant events. The need to spread attention across different
75   swaths of the visual field is driven, to a large degree, by spatial uncertainty: statistical
76   regularities give us a general sense as to where something useful might happen, and this
77   evolves from moment to moment. We navigate this uncertainty by dynamically deploying
78   spatial attention.

79   Covert spatial attention improves behavioral performance at attended locations
80   at the cost of performance at unattended locations (Posner, 1980), leading to a common
81   metaphor that spatial selective attention acts as a 'spotlight' or 'zoom lens' (Shaw and
82   Shaw, 1977; Posner, 1980; Eriksen and St. James, 1986; Carrasco, 2011). This
83   attentional 'spotlight' is characterized by a specific size and location and traverses the
84   visual field based on behavioral demands (Eriksen and St. James, 1986; Castiello and
85   Umiltà, 1990), selectively boosting information at the attended location within the visual
86   system while suppressing information elsewhere. Animal studies have observed
87   multiplicative increases in visuocortical neural responses at attended locations
88   (McAdams and Maunsell, 1999; Maunsell, 2015) and human neuroimaging studies have
89   found similar focal enhancements of population responses (Kastner *et al.*, 1998;
90   Brefczynski and DeYoe, 1999; McMains and Somers, 2004; Datta and DeYoe, 2009;
91   Sprague and Serences, 2013; Puckett and DeYoe, 2015; Samaha, Sprague and Postle,
92   2016; Shioiri *et al.*, 2016; Bloem and Ling, 2019).

93   While neural modulation at the locus of attention has been relatively well studied,
94   less is known regarding the neural signatures of the size of the attentional field
95   (Yeshurun, 2019). Spreading attention over a larger region of visual space can decrease
96   behavioral performance, but only a handful of studies have interrogated associated
97   effects within visual cortex (Müller *et al.*, 2003; Herrmann *et al.*, 2010; Itthipuripat *et al.*,
98   2014; Feldmann-Wüstefeld and Awh, 2020). This is surprising, as the spatial distribution
99   of the attentional field is a key feature in an influential theoretical model of attention
100   (Reynolds and Heeger, 2009). The model assumes that the size of the attentional field
101   can be adjusted based on task demands and that the interaction between attentional
102   field size and stimulus-related factors can predict observed attentional gain effects.

103   While the studies that have experimentally manipulated the attentional field size
104   found evidence congruent with this prominent theory (Herrmann *et al.*, 2010; Itthipuripat
105   *et al.*, 2014; Kınıklıoğlu and Boyaci, 2022), few studies have directly investigated the
106   spatial extent of the attentional window and its concomitant neural representation. One
107   neuroimaging study revealed that the attentional field expanded in the face of greater
108   task-related uncertainty (Herrmann *et al.*, 2010), while other studies showed that the
109   responsive area of visual cortex increased in size, coupled with a decrease of the overall
110   population response (Müller *et al.*, 2003; Feldmann-Wüstefeld and Awh, 2020). While
111   these studies are consistent with the notion that the attentional field size can be detected

112   in visual cortex, methods for dynamically recovering location and field size from moment
113   to moment are lacking.
114   In this study, we developed a paradigm that allowed us to dynamically
115   characterize the spatial tuning of spatial attention across the visual field. Using fMRI in
116   humans, we examined whether attentional modulation of the BOLD response spanned
117   a larger area of visual cortex when participants were cued to perform attend to a larger
118   region of space. Behavioral performance confirmed that participants could successfully
119   allocate their attention to different-sized swaths of the visual field. This deployment of
120   attention was associated with a boost in cortical activity in the corresponding retinotopic
121   areas of visual cortex. By modeling the location and spread of the visuocortical
122   modulation, we dynamically recovered the cued location from the attentional activity with
123   a high degree of fidelity, together with a broadening of the attentional enhancement for
124   wider attentional cues.

1 Materials and Methods

2 ***Participants.*** Eight healthy adults (4 female, 4 male, mean age = 30) participated in the
3 main attention experiment, five of whom also participated in a second experiment
4 featuring a contrast manipulation. All participants had normal or corrected-to-normal
5 vision. All procedures were approved by the Boston University Institutional Review
6 Board, and informed consent was obtained from all participants.

7

8 ***Apparatus and stimuli.*** Participants were presented with stimuli generated using
9 PsychoPy (v1.85.1; Peirce, 2007) on a MacBook Pro. The visual stimuli were displayed
10 on a rear-projection screen (subtending ~20°x16° visual angle) using a VPixx
11 Technologies PROPixx DLP LED projector (maximum luminance 306 cd/m^2).
12 Participants viewed the screen through a front surface mirror. Participants were placed
13 comfortably in the scanner with padding to minimize head motion.

14

15 ***Procedure.***
16 *Attentional width manipulation.* Participants were instructed to fixate a central point
17 (radius 0.08° visual angle) while dynamic pixelwise white noise (flickering at 10 Hz, 50%
18 contrast) was presented in the periphery (annulus spanning 4.6° to 7.4° visual angle).
19 The annulus was segmented into 20 bins (18° polar angle per bin) by white grid lines
20 radiating from a white circle at the center of the screen (radius 0.25°), passing behind
21 the annulus, and terminating at 8.5° eccentricity. In the middle of each bin, a number or
22 letter (height: 2.1°) was superimposed on the white noise annulus (see **Figure 1a**). For a
23 subset of the participants (3 out of 8) the screen distance inside the scanner was
24 changed, therefore for those participants the letter size was 1.86° visual angle, and the
25 white noise annulus spanned 4.1° to 6.5° visual angle. The set of possible letters included
26 all lowercase letters of the Latin alphabet except a, b, e, g, i, o, and u. The set of numbers
27 included 2, 3, 4, 5, 7, and 8.
28 　　　Participants were cued to attend covertly to a contiguous subset of the bins and
29 their task was to report, via button press, whether there were more *numbers* or *letters*
30 present within the cued region. The cue was a bold red segment on the central white
31 circle, which corresponded to 1, 3, 5, or 9 bins (18°, 54°, 90°, or 162° polar angle; see
32 **Figure 1a**). The true proportion of letters versus numbers was controlled within each cue
33 width condition. For cued regions of 1 bin, there was either a single number or letter in
34 the bin. For cued regions of 3 bins, the ratio was always 2:1 (either two numbers and one
35 letter or vice versa). For cued regions of 5 bins, the ratio was 3:2, and for cued regions
36 of 9 bins, the ratio was 6:3. Cues could be centered on any of the 20 bins.
37 　　　Participants completed 8 to 12 runs of the task (mean = 10.4), with each run
38 lasting 341 s and containing 100 trials. Each cue remained constant for a block of five
39 trials (lasting 15.5 s, 10 TRs), although the letters and numbers within the cued region
40 changed on every trial. Thus, each participant saw 20 unique cues (combinations of cue
41 location and width) per run. Each run began and ended with 15.5 s of the dynamic noise
42 annulus.

43   During each trial, the cue and white noise annulus were presented alone for 1.35
44   s. The numbers and letters were then displayed for 0.5 s. Thereafter, the cue and white
45   noise remained visible while the participant had 1.25 s to indicate whether there had
46   been more digits or letters within the cued region, resulting in a total trial duration of 3.1
47   s (2 TRs). No accuracy feedback was provided during the main experiment. However, all
48   participants completed three training runs with trial-by-trial feedback prior to the scan
49   session. During training runs, the response window was shortened to 1 s and the
50   remaining 0.25 s presented feedback in the form of a change in color of the fixation point
51   (blue for correct responses and orange for incorrect responses).

52

53   *Physical contrast manipulation*. A subset of participants (n=5) also participated in an
54   experiment that enhanced the physical contrast intensity of the dynamic visual noise in
55   segments of the annulus. This additional experiment was carried out during the same
56   scan session and allowed for benchmarking the detectability of stimulus-evoked
57   modulation in visual cortex using our analyses. The stimuli and trial structure were similar
58   to the attentional manipulation. The task differed in the following ways: (1) the contrast
59   of the white noise annulus was increased to 100% for segments of the annulus
60   corresponding to 1, 3, 5, 7 or 9 bins (18°, 54°, 90°, 126°, or 162° polar angle), with a
61   Gaussian rolloff ($\sigma = 15°$) that spanned 25% of the furthest included bins and 25% of the
62   adjacent excluded bins; (2) the enhanced segments were always centered on the
63   cardinal directions (0°, 90°, 180°, and 270° polar angle); (3) the contrast increase
64   remained constant for 15.5 seconds (10 TRs); (4) participants performed a color change
65   detection task at fixation. Each unique combination of 4 locations and 5 widths of the
66   contrast enhancement was shown once per run, with the order randomized. To estimate
67   a baseline response, each run started and ended with 15.5 seconds without contrast
68   modulation. Participants completed two runs total, each lasting 341 seconds (220 TRs).
69   Throughout the *physical contrast* runs, participants were instructed to fixate on a
70   central point (radius 0.08° visual angle) and to press a button when the fixation point
71   switched color (alternating white and red). The fixation point remained a color for at least
72   one second and then had a 10% probability of switching every 100 ms. No cue was
73   presented associated with the regions of increased contrast. Additionally, no letters or
74   numbers were superimposed on the white noise annulus.

75

76   *Population receptive field mapping*. Population receptive field (pRF) estimates were
77   obtained for each participant in a separate scan session. We used the experimental
78   procedure as described in the Human Connectome Project 7T Retinotopy dataset
79   (Benson *et al.*, 2018). Stimuli were composed of a pink noise background with colorful
80   objects and faces at various spatial scales, displayed on a mean luminance gray
81   background. Stimuli were updated at a rate of 15 Hz while participants performed a color
82   change detection task at fixation. Participants viewed two types of mapping stimuli: (1)
83   contracting/expanding rings and rotating wedges; (2) moving bar stimuli (Dumoulin and
84   Wandell, 2008; Kay *et al.*, 2013). A total of 4-6 scans (300 TRs) were collected for each
85   participant (2-3 scans per stimulus type).

86

87   ***MRI data acquisition.*** All MRI data were acquired at Boston University's Cognitive
88   Neuroimaging Center (Boston, Massachusetts) on a research-dedicated Siemens
89   Prisma 3T scanner using a 64-channel head coil. A scanning session lasted 2 hours.
90   All functional neuroimaging data were acquired using a simultaneous multislice (SMS)
91   gradient echo echoplanar acquisition protocol (Moeller *et al.*, 2010; Setsompop *et al.*,
92   2012): 2 mm isotropic voxels; FoV = 212 x 212 mm; 72 axial slices; TR = 1.55 s; TE =
93   35.60 ms; flip angle = 72°; multiband acceleration factor 4. We computed distortion field
94   maps by using a spin echo echoplanar protocol with opposite y-axis phase encoding
95   directions (2 mm isotropic voxels; FOV = 212 x 212 mm; TR = 8850 ms; TE = 70.80 ms;
96   flip angle = 90°). During a separate scan session, we acquired a whole-brain anatomical
97   scan using a T1-weighted multi-echo MPRAGE 3d sequence (1 mm isotropic; FoV = 256
98   x 256 mm; 176 sagittal slices; TR = 2530 ms; TE = 1.69 ms; flip angle = 7°), and the pRF
99   scans (occipital coverage only; right-left phase encoding; 2 mm isotropic voxels; FoV =
100   136 x 136 mm; 36 slices; TR = 1 s; TE = 35.4 ms; flip angle = 64°; multiband acceleration
101   factor 3).

102

103   ***MRI data analysis.***
104   *Structural data preprocessing.* Whole brain T1-weighted anatomical data were analyzed
105   using the standard 'recon-all' pipeline provided by Freesurfer software (Freesurfer
106   version 5.3, (Fischl, 2012)), generating cortical surface models, whole-brain
107   segmentation, and cortical parcellations.

108

109   *Functional data preprocessing.* All analyses were performed in the native space for each
110   participant. First, EPI distortion correction was applied to all fMRI BOLD time-series data
111   using a reverse phase-encode method (Andersson, Skare and Ashburner, 2003)
112   implemented in FSL (Smith *et al.*, 2004). All functional data were then preprocessed using
113   FS-FAST (Fischl, 2012), including standard motion-correction procedures, Siemens slice
114   timing correction, and boundary-based registration between anatomical and functional
115   volumetric spaces (Greve and Fischl, 2009). To facilitate voxel-wise analysis, no
116   volumetric smoothing was performed and across-run within-modality robust rigid
117   registration was applied (Reuter, Rosas and Fischl, 2010), with the middle time-point of
118   the first run serving as the target volume, and the middle time-point of each subsequent
119   run used as a movable volume for alignment. Lastly, data were detrended (0.005 Hz
120   high-pass filter) and converted to percent signal change for each voxel independently
121   using custom code written in MATLAB (version 2020b).

122

123   *Population receptive field mapping and voxel selection.* The time series were analyzed
124   using the analyzePRF toolbox in MATLAB, implementing a compressive spatial
125   summation pRF model (Kay *et al.*, 2013). The results of the pRF analysis were used to
126   manually draw boundaries between early visual regions (V1, V2, and V3), which served
127   as our regions of interest (ROIs).
128   Within each ROI, pRF modeling results were used to constrain voxel selection
129   used in the main experiment. We excluded voxels with a preferred eccentricity outside
130   the bounds of the pRF stimulus (<0.7° and >9.1°), with a pRF size smaller than 0.01°, or
131   with poor spatial selectivity as indicated by the pRF model fit ($R^2 < 10\%$). Following our

132   2D visualizations (see below), we further constrained voxel selection by only including
133   voxels whose pRF overlapped with the white noise annulus.

134

135   *2D visualizations of attentional modulation*. To visualize the topography of attentional
136   modulation under different cue widths, we projected the average BOLD responses for a
137   given block (10 TRs with a consistent cue location and width, shifted by 3 TRs [4.65 s]
138   to compensate for the hemodynamic delay) into the visual field using each voxel's pRF
139   location. This method is similar to that described in (Favila, Kuhl and Winawer, 2022).
140   First, we computed the Cartesian (x,y) coordinates from the pRF eccentricity and polar
141   angle estimates for each voxel. Then, within a given ROI, we interpolated the BOLD
142   responses over (x,y) space to produce a full-field representation. Each representation
143   was then z-scored to allow for comparison across blocks, cue conditions, and
144   participants. Finally, the representation was rotated so that the center of the cue was
145   aligned to the right horizontal meridian (see **Figure 2a**).

146

147   *1D spatial profile of attentional modulation.* We also examined the spatial profile of
148   attentional modulation as a function of polar angle. Voxels with pRFs overlapping the
149   white noise annulus were grouped into 60 bins according to their pRF polar angle
150   estimate (6° polar angle bin width). We computed a median BOLD response within each
151   bin. To improve the signal-to-noise ratio, the resulting profile was smoothed with a
152   moving average filter (width 18° polar angle; see **Figure 2b**).

153

154   *Model fitting.* We quantified the spatial profile of attentional modulation with a
155   generalized Gaussian model (Nadarajah, 2005). The generalized Gaussian function (G)
156   combines Gaussian and Laplace distributions:

$$G = exp\left\{-\left|\frac{x-\mu}{\sigma}\right|^{\beta}\right\} \tag{1}$$

157   The function has free parameters for location (μ), scale (σ), and shape (β). The shape
158   parameter enables the tails of the distribution to become heavier than Gaussian (when
159    $\beta < 2$), or lighter than Gaussian (when $\beta > 2$); as $\beta \to \infty$, the model approaches a
160   uniform distribution.

161

162   Next, G was normalized to range between 0 and 1, and vertically scaled and shifted by
163   two additional free parameters for amplitude (a) and baseline offset (b):

$$\hat{y} = a \cdot G + b \tag{2}$$

164   We fit the five free parameters (μ, σ, β, a, b) using the MATLAB optimization tool *fmincon,*
165   minimizing the squared error between the model prediction and the 1D profile described
166   above. To avoid local minima, we first ran a grid search to find the initialization values
167   with the lowest SSE (6 possible values for μ, equally spaced between 0 and 360°,

168   crossed with 6 possible values for σ, equally spaced between 9° and 162° polar angle;
169    $\beta = 4$; $a = 1$; $b = 0$). We imposed the following parameter bounds on the search: σ: [6°,
170   180° polar angle], β: [1.8, 50], and a: [0, 20]. μ was unbounded, but was wrapped to
171   remain within [0°, 360°].
172   From the model fits we computed the following summary metrics: 1) angular error,
173   defined as the polar-angle distance between the true and estimated location; 2) the full
174   width at half-maximum (FWHM) of the best-fitting generalized Gaussian function, which
175   served as our measure of the width of attentional modulation. The FWHM was controlled
176   mainly by the scale parameter (σ) but also to a lesser degree by the shape parameter (β;
177   see **Figure 3a**); 3) the gain modulation of the spatial profile (a); 4) the model's goodness
178   of fit quantified as the percentage of explained variance (R^2) in the spatial response
179   profile:

$$R^2 = 1 - \frac{(y - \hat{y})^2}{(y - \bar{y})^2} \tag{3}$$

180   ***Statistical testing***. To assess how the attentional cue width manipulation influenced the
181   1D spatial profile of BOLD modulation, we tested whether the computed summary
182   metrics (absolute angular error, FWHM, and amplitude) varied as a function of cue width.
183   Specifically, we performed a linear regression for each metric and tested whether the
184   slopes differed from zero. This was done independently for each ROI.
185
186   ***Eye-position monitoring***. Gaze data were collected for all participants using an MR-
187   compatible SR Research EyeLink 1000+ eye tracker sampling at 1 kHz. Data from blink
188   periods were excluded from analysis. Participants maintained fixation throughout the
189   task, with average gaze eccentricity below 0.5° for all participants. Gaze eccentricity did
190   not significantly vary by cued width (pairwise comparison of width conditions using a
191   paired t-test, all $p >= 0.205$ with Bonferroni correction for multiple comparisons) nor
192   location (pairwise comparison, all $p >= 0.522$ with Bonferroni correction for multiple
193   comparisons).

1 Results

2 Behavioral performance indicates effective deployment of covert spatial attention

3   We set out to investigate the spatial distribution of attentional modulation within
4 visual cortex. To do so, we first ensured that participants (*n*=8) could successfully
5 allocate covert spatial attention to cued portions of the visual field. During the
6 experiment, participants' task was to fixate the center of the screen and report whether
7 there were more *numbers* or *letters* in a cued peripheral region (**Figure 1a**). The cued
8 region varied in location and width: it could be centered on any of 20 polar angles and
9 could span any of four widths (18°, 54°, 90°, and 162° of polar angle). Task performance
10 indicated that participants used the cue effectively, as the proportion of correct
11 responses was significantly above chance for all width conditions (**Figure 1b**; t-test, all
12 p<.001). We verified, with eye tracking, that participants performed the task using
13 peripheral vision while maintaining central fixation. The upper bound of the 95% CI for
14 each participant's average gaze eccentricity ranged from 0.29° (degrees of visual angle)
15 to 0.64° (mean = 0.48°; **Figure 1c**), suggesting that gaze did not exceed the cue annulus
16 at fixation and that participants used covert spatial attention to perform the task.
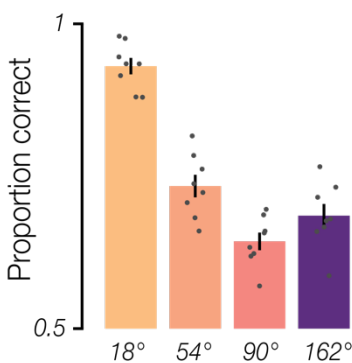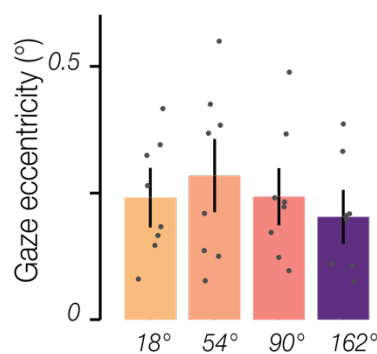

a. Attention task trial sequence

b. Behavioral task performance

c. Gaze distance from fixation

Figure 1. a. Task schematic. Participants' were instructed to maintain central fixation and use covert spatial attention to determine whether there were more numbers or letters present within a cued region of a white noise annulus. On each trial, the red cue was displayed alone for 1.35 s and remained present throughout the trial. Twenty digits and letters were then presented for 0.5 s, equally spaced and overlaid on the annulus. Participants had 1.25 s to indicate via button press whether more digits or letters were present in the cued region. The cue remained stable for 5 trials (10 TRs, 15.5 s), had a width of 1, 3, 5, or 9 segments (18°, 54°, 90°, or 162°), and was centered on any of the 20 digit/letter slots. **b.** Behavioral task performance: Group mean accuracy for each cue width. Error bars are SEM; gray circles show individual participants. **c.** Group mean gaze eccentricity (in degrees of visual angle) for each cue width, conventions as in **b**.

Attentional modulation of BOLD responses broadens with cue width

17

18   We assessed the spatial distribution of attention by visualizing how the BOLD
19 response was modulated by the location and width of the cue. To do so, we used each
20 voxel's population receptive field (pRF) to project BOLD responses for each attentional
21 cue into the visual field. The resulting 2D visual field maps were averaged across trials
22 for each cue width by rotating the maps so the attentional cue aligned to 0° polar angle
23 (right horizontal meridian). The reconstructed visual field maps revealed that increasing
24 cue width led to a concomitant broadening of attentional modulation in cortex (**Figure
25 2a**). While this pattern was evident in all three early visual regions (V1–V3), the effect
26 appeared to strengthen when ascending the visuocortical hierarchy.

27   Next, we computed the one-dimensional profile of attentional modulation at a
28 fixed eccentricity. We were able to do this because we manipulated the location of the
29 attentional field only as a function of polar angle, so all cues directed the attentional field
30 to iso-eccentric locations. We selected voxels with pRFs that overlapped the white noise
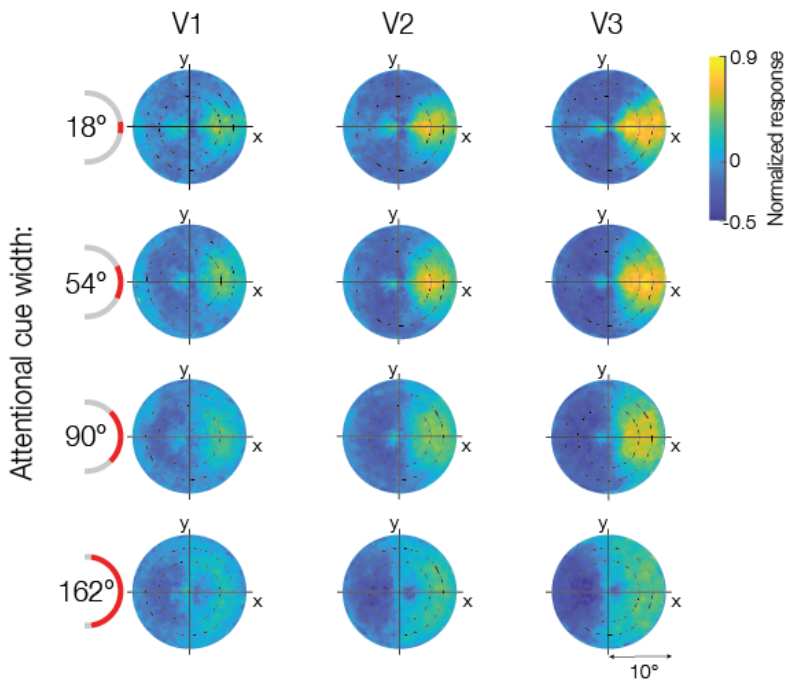31 annulus and sorted them according to their polar angle preference.

Figure 2. a. BOLD response projected into the visual field for each attentional cue width. Heatmaps represent the group mean BOLD activity using each voxel's population receptive field (pRF) location within the visual field, shown separately for V1, V2, and V3. Maps were rotated to align all attentional cue locations to 0° polar angle (rightward). Concentric circles indicated by black dashed lines represent the location of the white noise annulus. **b.** Average spatial modulation profiles at the eccentricity of the annulus. The spatial profiles were recentered to 0° polar angle based on the cue location. Solid lines represent the group mean BOLD activity and shaded regions the SEM across participants.
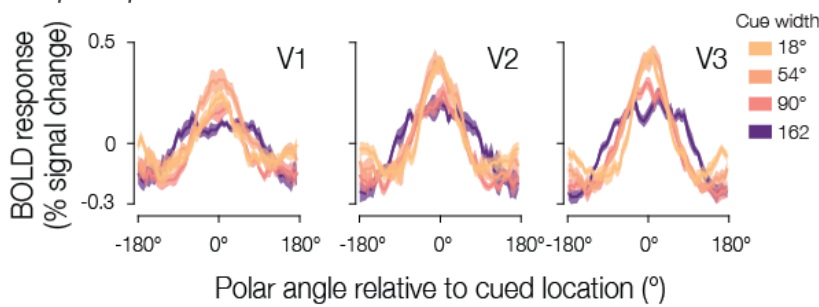
32   For visualization purposes, the spatial response modulations were recentered to
33   align all cues at 0° polar angle and averaged across trials for each cue width separately.
34   Much like in the visual field reconstructions, there was a clear attentional enhancement
35   centered on 0°, which broadened and decreased in amplitude with cue width – a pattern
36   that was particularly evident in area V3 (**Figure 2b**).

37   **Dynamic model-based recovery of the attentional field**
38   We next applied a modeling approach to estimate the location and width of
39   attentional modulation, allowing us to further investigate the spread of attention in visual
40   cortex. To do this, we averaged the spatial response profiles across TRs within each 10-
41   TR block, in which the cue maintained a consistent location and width, yielding between
42   27 and 53 averaged spatial response profiles per participant for each width condition.
43   We fit a generalized Gaussian function to each of these spatial profiles to estimate the
44   location and width of attentional modulation per spatial profile (see **Figure 3a**). The width
45   of attentional modulation was quantified in terms of the full width at half maximum
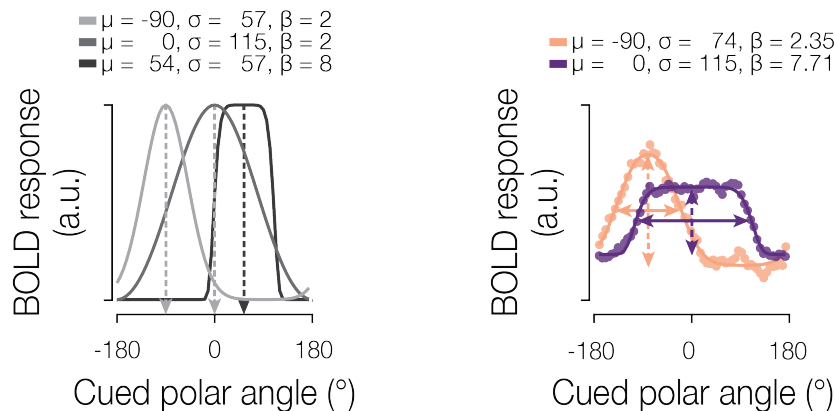46   (FWHM) of the best fitting model prediction (see **Figure 3b**).

Figure 3. **a.** Modeling approach. The generalized Gaussian model is characterized by parameters for location (μ), scale (σ), and shape (β). **b.** Example model fits for two spatial profiles. Dots indicate BOLD response amplitudes for two attentional cues differing in position and width. Solid lines indicate the best fitting model estimate. To quantify the attentional field, we extracted the location and gain (dashed arrows), as well as the width (FWHM; solid arrows).

47   Can we dynamically recover the attentional field from activity within visual cortex?
48   Model fits explained a substantial proportion of variance in the spatial profiles of BOLD
49   activity (**V1**: for 18° cues, mean [standard deviation] of R^2 = 0.42 [0.03]; for 54° cues, 0.43
50   [0.03]; for 90° cues, 0.44 [0.03]; for 162° cues, 0.42 [0.03]; **V2**: for 18° cues, 0.51 [0.05];
51   for 54° cues, 0.54 [0.05]; for 90° cues, 0.54 [0.04]; for 162° cues, 0.55 [0.04]; **V3**: for 18°
52   cues, 0.50 [0.03]; for 54° cues, 0.56 [0.04]; for 90° cues, 0.55 [0.03]; for 162° cues, 0.51
53   [0.02]). To interpret the estimated model parameters, we excluded the bottom 20% of
54   fits based on a pooled R^2 across V1, V2, and V3, leaving roughly equal proportions of
55   included blocks across cue width conditions (18°: mean [standard deviation] = 0.78
56   [0.04], 54°: 0.83 [0.05], 90°: 0.83 [0.04], 162°: 0.77 [0.07]).

57   To assess how well the model-estimated attentional field matched the cued
58 location, we first calculated the angular error between the cue center and the model's
59 estimated location parameter. The angular error distribution across blocks, separated by
60 width condition, is shown in **Figure 4a** for one example participant to display block-to-
61 block variation. The model reliably captured the location of the attentional field with low
62 angular error. This result was consistent across participants. The group mean absolute
63 angular error in V1 was 41.9° (SEM=2.86°), in V2 was 32.2° (2.31°), and in V3 was 24.7°
64 (1.54°). Additionally, the magnitude of the absolute error did not vary linearly with the
65 width of the cue in V1 or V2 (regression slope tested against zero; both *p*>=.468; **Figure
66 4b**). In V3, we observed a small but statistically significant increase in absolute error
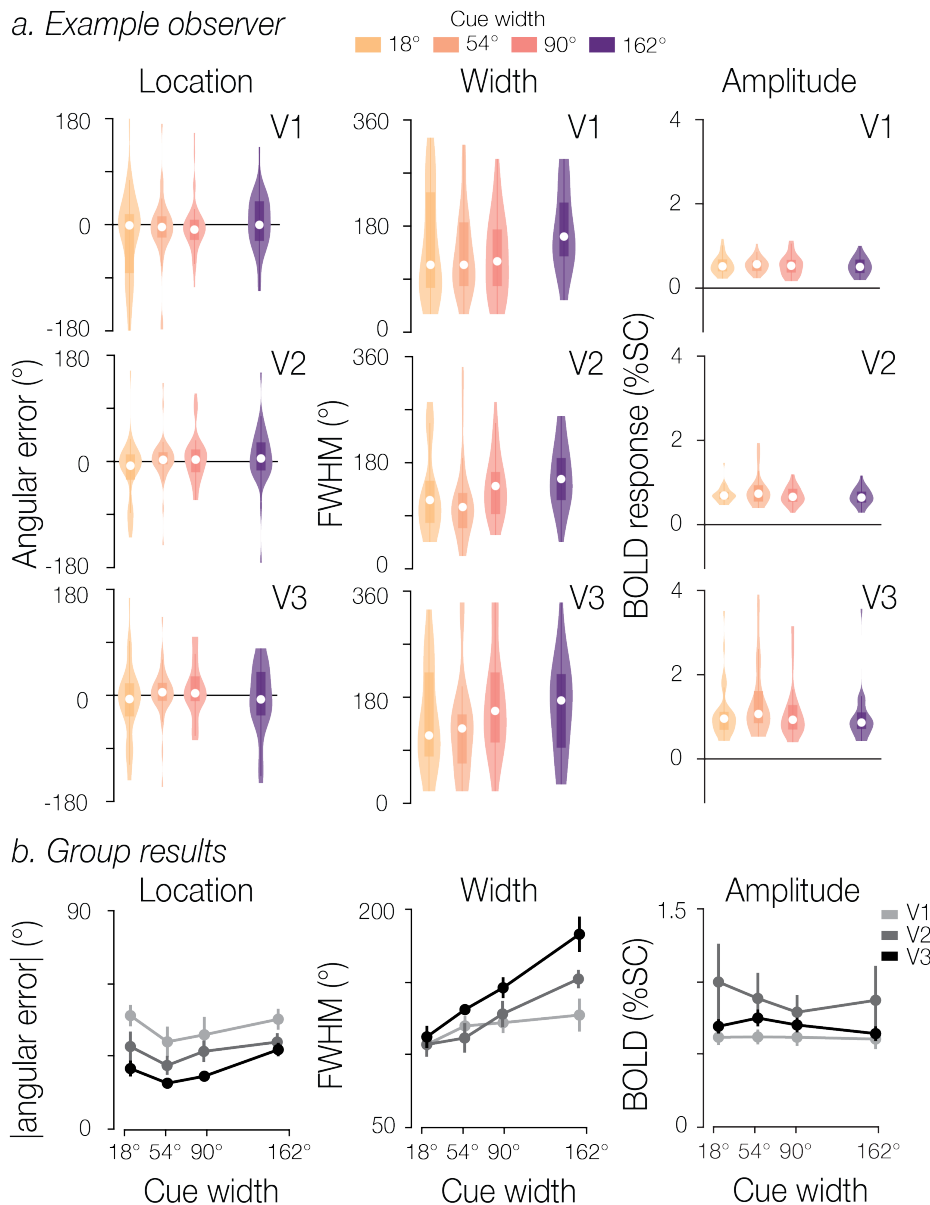67 magnitude associated with greater cue widths ($t(1,30)=2.86$, *p*=.008).

Figure 4. Attentional field parameter estimates. **a.** The full parameter estimate distributions across blocks for location, width, and amplitude are shown for one example participant in V1, V2, and V3. Median parameter estimates are shown by the white points, with the box plot representing the 25th to 75th percentile, and whiskers extending to all non-outlier points. **b.** Group results for location, width, and amplitude estimates. Overall group mean and standard error are shown, separated by cue width and brain region.

68   Next, we evaluated the width of the attentional field by visualizing the distribution
69 of FWHM for the same example participant (**Figure 4a**), and at the group level (**Figure**
70 **4b**). Confirming the broadening of the attentional field observed in the visual field
71 reconstruction maps, we found that the estimated FWHM increased with greater cue
72 widths in V2 and V3 (V2 $t(1,30)=4.60$, $p<.001$; V3 $t(1,30)=6.71$, $p<.001$). The effect was
73 not statistically significant in V1 ($t(1,30)=1.61$, $p=.118$).
74   Finally, we assessed the gain of the attentional modulation in the model (**Figure**
75 **4a** and **4b** for the example participant and group data, respectively). We observed no
76 significant relationship between amplitude and cue width (V1 $t(1,30)=-.18$, $p=.861$; V2
77 $t(1,30)=-.42$, $p=.677$; V3 $t(1,30)=-1.00$, $p=.325$). We also found that the overall gain was
78 greater in V2 and V3 compared to V1 (paired t-test, both $p<=.01$).

79 **Temporal interval analysis**

80   In the previous analyses, we leveraged the fact that the attentional cue remained
81 constant for 5-trial blocks (spatial profiles were computed by averaging BOLD
82 measurements across a block of 10 TRs). We next examined the degree to which we
83 were able to recover the attentional field on a moment-by-moment (TR-by-TR) basis. To
84 examine the consistency of the attentional field over a varying number of TRs with an
85 identical cue, we systematically adjusted the number of TRs that contributed to the
86 averaged spatial response profile. To maintain a constant number of observations across
87 the temporal interval conditions, we randomly sampled a subset of TRs from each block.
88   When we systematically varied the number of TRs included for each model fit (1,
89 2, 3, 5, or 10 TRs), we found a significantly positive linear relationship between cue width
90 and recovered FWHM when averaging two or more TRs in V3 (all $p<=.008$), and five or
91 more TRs in V2 (both $p<=.034$; **Figure 5a**). As described above, V1 did not reliably show
92 a monotonic relationship between cue width and FWHM, even when averaging ten TRs.
93 We did not find that varying the number of TRs systematically altered the FWHM
94 estimates in V1 or V3 (V1, $t(1,18)=1.70$, p=.106; V3, $t(1,18)=.85$, p=.405), although a
95 significant effect was observed in V2 such that larger numbers of TRs were associated
96 with greater width estimates ($t(1,18)=2.39$, p=.028).
97   The number of TRs significantly affected the absolute angular error associated
98 with the estimated location of the attentional field **(Figure 5b)**. Error magnitude
99 decreased with TRs in all three visual regions (V1, $t(1,18)=-4.40$, p<.001; V2, $t(1,18)=-$
100 5.15, p<.001; V3, $t(1,18)=-4.10$, p<.001), suggesting that more data yielded more
101 accurate estimates, though absolute angular error remained consistently below chance
102 (90°) even when fitting the model to single-TR BOLD responses. Location error remained
103 stable across width conditions (V1, $t(1,18)=-.38$, p=.706; V2, $t(1,18)=.66$, p=.520; V3,
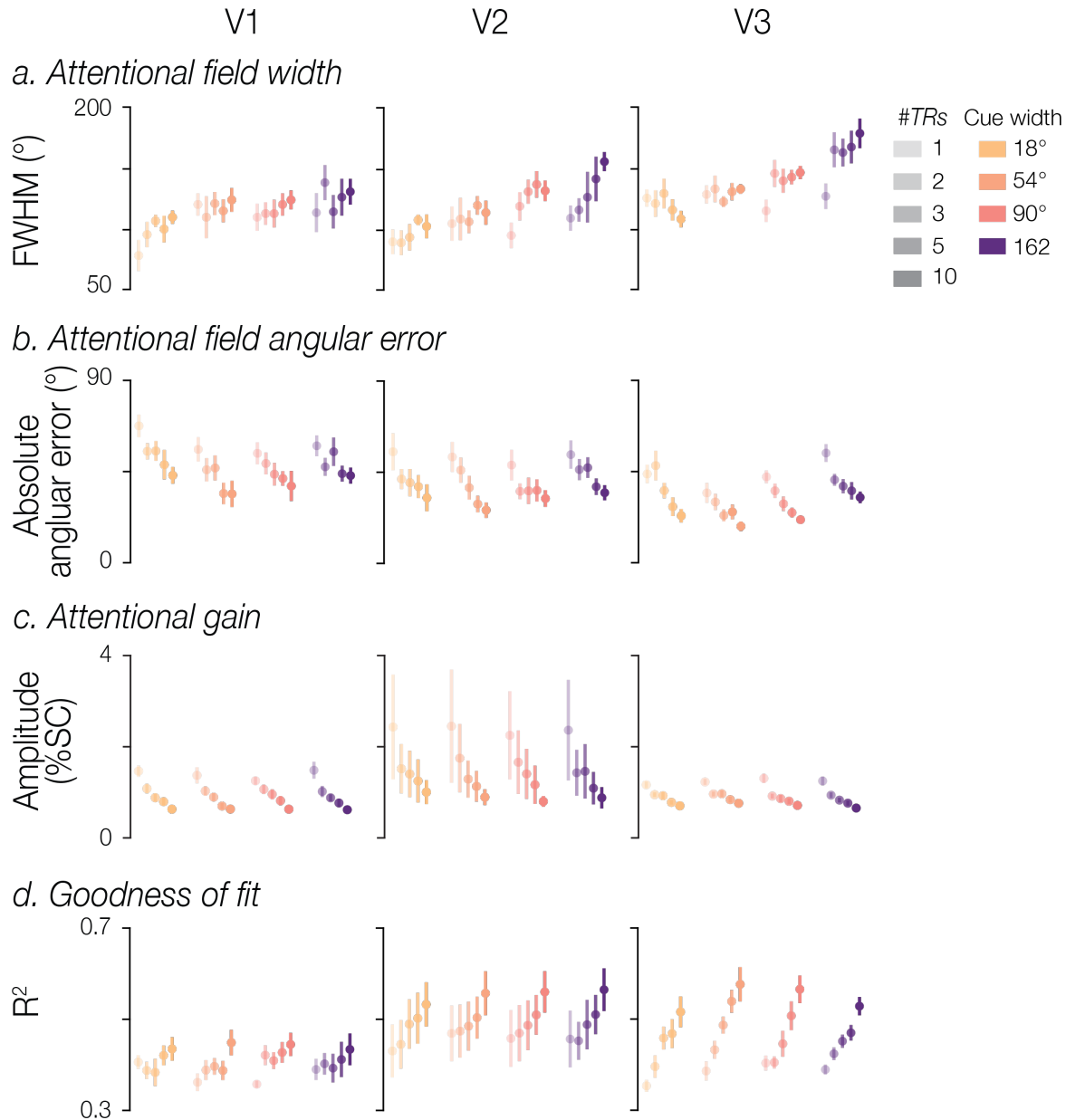104 $t(1,18)=1.29$, p=.215).

Figure 5. Effect of number of TRs. Model fits were computed using BOLD data averaged across different temporal intervals (1, 2, 3, 5, or 10 TRs). Group means (with SEM) are plotted for FWHM, absolute angular error, amplitude estimates, and R^2, separated by cue width, brain region, and the number of TRs used for each model fit.

105   The estimated gain of the attentional enhancement showed a dependence on number of TRs, with more TRs associated with lower gain estimates (V1, $t(1,18)=-6.67$, $p<.001$; V2, $t(1,18)=-6.03$, $p<.001$; V3, $t(1,18)=-5.74$, $p<.001$), with no evident dependence on cue width (V1 $t(1,18)=-.03$, $p=.976$; V2 $t(1,18)=-.24$, $p=.810$; V3 $t(1,18)=-.28$, $p=.782$; **Figure 5c**).

110   Finally, the model's goodness of fit improved with more data, with larger R^2 associated with greater numbers of TRs included in the average profiles (V1, $t(1,18)=5.82$, $p<.001$; V2, $t(1,18)=12.89$, $p<.001$; V3, $t(1,18)=8.30$, $p<.001$), though all R^2 were above 0.3 across all visual regions even for single-TR model fits. We did not

114   observe a dependence of R^2 on cue width (V1, $t(1,18)=.23$, $p=.823$; V2, $t(1,18)=.46$,
115    $p=.653$; V3, $t(1,18)=.05$, $p=.959$; **Figure 5d**).

Width of the attentional field mimics perceptual modulation

117   While the attentional field broadened as expected when participants were cued
118   to attend to a larger portion of the white noise annulus, the size of the estimated
119   attentional modulation was greater than the true size of the cued region. The cue width
120   varied between 18° and 162°, whereas the width estimate derived from spatial profiles
121   of BOLD modulation varied between 103° and 179° (**Figure 4b**). We wondered what the
122   underlying cause of this disparity might be. One possibility is that the BOLD-derived
123   FWHM might tend to overestimate the retinotopic extent of the modulation. If this were
124   the case, we would expect to obtain overestimates of FWHM when applying the same
125   modeling approach to perceptual modulations as well. Alternatively, the true subjective
126   attentional field might be consistently broader than cued, despite the presence of nearby
127   distractors. If this were the case, modulation driven by perceptual differences should *not*
128   result in the same large FWHM estimates.
129   To address this, we compared our estimates of the attentional field with
130   equivalent estimates for spatial profiles induced by a perceptual manipulation. In this
131   additional experiment, we varied the contrast intensity of sections of the white noise
132   annulus. Participants were not asked to deploy spatial attention to the stimulus and were
133   instead instructed to perform a color change detection task at fixation. The regions of
134   increased noise contrast matched the attentional cue widths (18°, 54°, 90°, and 162°,
135   plus an additional intermediate width of 126º), and were centered on one of the four
136   cardinal locations (0°, 90°, 180°, 270° polar angle).
137   As expected, we observed a broadening of the spatial profile of BOLD modulation
138   in all three visual areas as the region of increased contrast widened (**Figure 6a**). Using
139   an identical modeling procedure, we estimated the spatial profile of the *perceptual* BOLD
140   modulation. The group results for model estimates revealed that: 1) we were highly
141   accurate in estimating the location of the contrast increment; 2) FWHM of the spatial
142   profiles broadened across contrast widths, and 3) the amplitude remained stable across
143   contrast widths (**Figure 6b**).
144   Mirroring the results from the attentional manipulation, FWHM estimates
145   systematically exceeded the nominal size of the perceptually modulated region of the
146   visual field. Comparing the estimated FWHMs of the perceptual and attentional spatial
147   profiles (**Figure 6c**) revealed that the estimated widths were highly comparable (Pearson
148   correlation r=0.664 across width conditions and visual regions). This finding implies that
149   the BOLD-derived generative Gaussian model may have had a general tendency to
150   return upwardly biased width estimates, but that it recovered relative differences in a
151   similar manner for attentional and perceptual forms of modulation.
152   For the perceptual contrast manipulation, the increase in the recovered FWHM
153   with contrast width was observed in both V1 and V3 (**Figure 6b**; V1, $t(1,23)=4.59$, $p<.001$;
154   V3, $t(1,23)=4.96$, $p<.001$), though this effect was not clearly observed in V2 ($t(1,23)=1.22$,
155    $p=.236$). The mean magnitude of angular error between the model-estimated location
156   and the center of the contrast stimulus did not depend linearly on contrast width in any
157   of the three visual areas (all $p>=.584$). The estimated amplitude of modulation also did

158   not show a relationship to contrast width in any of the visual areas (V1, $t(1,23)=1.19$,
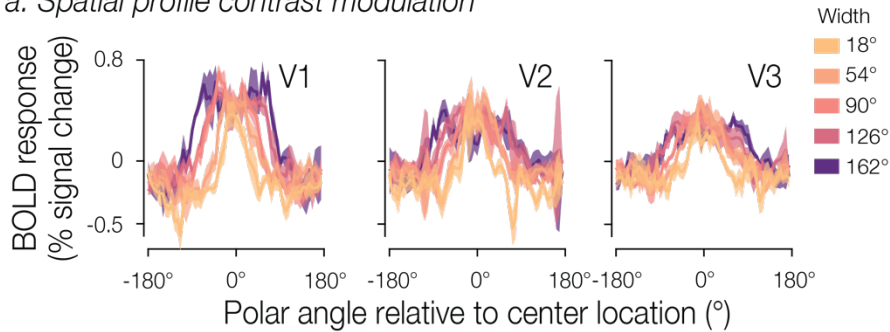159 $p=.245$; V2, $t(1,23)=-.32$, $p=.749$; V3, $t(1,23)=.28$, $p=.783$).
160

Figure 6. a. Spatial profiles of perceptual modulation. Solid lines represent the group mean BOLD activity and shaded regions the SEM. b. Group level parameter estimates. Overall group mean and standard error are shown for the absolute angular error, FWHM, and amplitude, separated by contrast width and brain region. c. Comparison of FWHM estimates obtained from the attentional manipulation and the physical contrast manipulation. Dot color indicates brain region; each point represents the mean FWHM for a given width condition across participants.
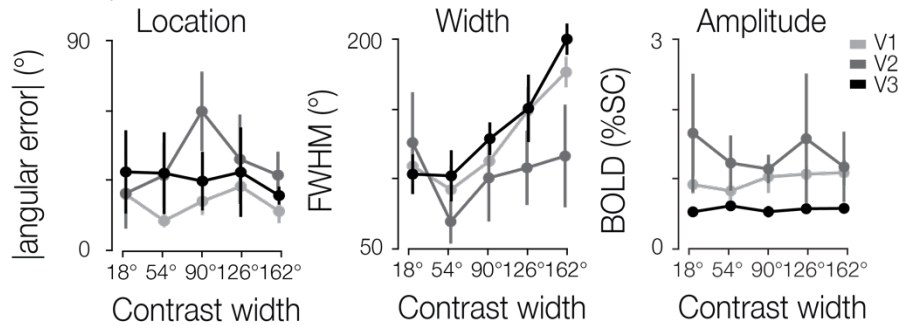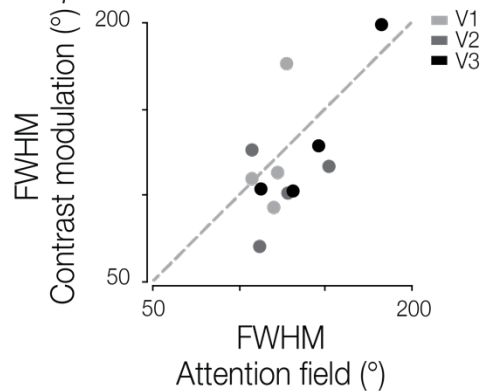
1 Discussion

2   We investigated the topographic spread of spatial attention in human visual cortex
3 by characterizing the spatial profile of BOLD responses while participants attended to
4 different portions of the visual field. Behavioral performance confirmed that participants
5 used the fixation cue to dynamically allocate attention to different swaths of the visual
6 field. Attention allocation was associated with a boost in the BOLD response in
7 corresponding retinotopic areas of visual cortex. To characterize the topography of that
8 boost, our approach involved selecting voxels with pRF preferred eccentricities that
9 overlapped our white noise annulus, and organizing those voxels into one-dimensional
10 profiles of attentional modulation as a function of preferred polar angle. This allowed us
11 to model the location and spread of the attentional field and test how well it tracked the
12 nominal location and width of the cue presented at fixation. Using a generalized
13 Gaussian model, the cued location could be recovered with high fidelity. Furthermore,
14 we observed a broadening of the estimated attentional field in areas V2 and V3 with the
15 cue width, suggesting our method was capable of dynamically recovering the location
16 and size of the attentional field from moment to moment.

17   This work builds on the concept of an attentional 'spotlight' or 'zoom lens' that
18 has long been theorized to aid in spatial attention (Shaw and Shaw, 1977; Posner, 1980;
19 Eriksen and St. James, 1986; Carrasco, 2011). By flexibly adjusting and shifting the focus
20 of the spotlight, visual representations are selectivity enhanced within a specific region
21 of the visual field. However, the empirical evidence demonstrating that attention can
22 change its *spread* across the visual field by modulating brain responses is surprisingly
23 lacking (Yeshurun, 2019). Our understanding of how the attentional window interacts
24 with spatial representations is mainly based on behavioral reports (Gobell, Tseng and
25 Sperling, 2004; Palmer and Moore, 2009; Herrmann *et al.*, 2010; Beilen *et al.*, 2011;
26 Taylor *et al.*, 2015; Huang *et al.*, 2017; Kınıklıoğlu and Boyaci, 2022), but see (Hopf *et al.*,
27 2006; Itthipuripat *et al.*, 2014; Tkacz-Domb and Yeshurun, 2018; Feldmann-Wüstefeld
28 and Awh, 2020), despite it forming a crucial component in an influential theoretical model
29 of attention (Reynolds and Heeger, 2009). This model proposes that the interaction
30 between stimulus properties (such as its size and specific features) and the attentional
31 field can explain a wide variety of attentional effects reported in behavioral and
32 neurophysiological studies (Herrmann *et al.*, 2010; Itthipuripat *et al.*, 2014; Bloem and
33 Ling, 2019; Jigo, Heeger and Carrasco, 2021). The present study sought to address this
34 gap, with our results showing that the visuocortical attentional field broadened as we
35 increased the cue width (**Figure 4**). This provides compelling evidence that the attention-
36 related cortical response can, in fact, flexibly vary in its position and spatial distribution.

37   In this study, we modeled the attentional field using a one-dimensional
38 distribution. This approach aligned with our experimental design, as the attentional cue
39 was manipulated only as a function of polar angle. However, we know that spatial
40 processing varies substantially as a function of eccentricity. Spatial resolution is highest
41 at the fovea and rapidly drops in the periphery (Anton-Erxleben and Carrasco, 2013). The
42 spatial distribution of attention will presumably also vary with eccentricity and will likely

43 take on different functional properties close to the fovea, where spatial resolution is high,
44 compared to the far periphery where spatial resolution is low (Intriligator and Cavanagh,
45 2001; Jigo, Heeger and Carrasco, 2021). Future work can help provide a better
46 understanding of the contribution of spatial attention by considering how the attentional
47 field interacts with these well described spatial variations across the visual field.
48 Measuring the full spatial distribution of the attentional field (across both eccentricity and
49 polar angle) will shed light on how spatial attention guides perception by interacting with
50 the non-uniformity of spatial representations.

51 The spread of the attentional field likely influences the degree to which spatial
52 resolution at the attended location is transformed, leading to enhanced behavioral
53 performance. In our experiment, we cued participant to varying swaths of an iso-
54 eccentric annulus of white noise and participants had to discriminate whether more
55 numbers or more letters were presented within the cued region. Spatial attention was
56 vital for this task, as enhanced spatial perception allowed the participants to better
57 discriminate all stimuli within the cued region (Anton-Erxleben and Carrasco, 2013).
58 However, the estimated spatial spread of the attentional modulation (as indicated by the
59 recovered FWHM) was consistently wider than the cued region itself. We therefore
60 compared the spread of the attention field with the spatial profile of a *perceptually*
61 induced width manipulation. Our model overestimated the retinotopic extent of the cued
62 region in both the attentional and perceptual versions of the task (**Figure 6c**), suggesting
63 that the BOLD-derived FWHM systematically overestimated the extent of modulation.
64 Future work could unpack the degree to which the size of the attentional field influences
65 the spatial resolution of visual cortical representations (Klein, Harvey and Dumoulin,
66 2014; Vo, Sprague and Serences, 2017; Tünçok, Carrasco and Winawer, 2024), and how
67 this influences spatial perception.

68 Beyond addressing core questions related to the function of spatial attention, this
69 method also lays groundwork for addressing questions about spatial predictive
70 uncertainty and belief updating. Prior work on these topics has relied almost entirely on
71 inferring participants' predictions from their behavior, often requiring participants to
72 report overt point predictions (Nassar *et al.*, 2010; McGuire *et al.*, 2014; D'Acremont and
73 Bossaerts, 2016; Nassar, Bruckner and Frank, 2019), or inferring participants'
74 predictions from their sequences of decisions (Daw *et al.*, 2006; Behrens *et al.*, 2007;
75 Payzan-LeNestour and Bossaerts, 2011; Payzan-LeNestour *et al.*, 2013). These
76 approaches have shed light on how we dynamically adapt our learning and belief
77 updating processes over time in differently structured contexts. However, methods for
78 recovering information about full predictive belief distributions have been limited, relying
79 on indirect measurements such as eye movements (O'Reilly *et al.*, 2013; Bakst and
80 McGuire, 2021, 2023), and physiological measures of uncertainty and surprise in EEG
81 and pupillometry (Preuschoff, 't Hart and Einhauser, 2011; Nassar *et al.*, 2012; Nassar,
82 Bruckner and Frank, 2019). The methods developed here offer a potential way to recover
83 the location and width of a spatial predictive distribution via the attentional field in
84 contexts in which it is unknown *a priori* and might be dependent on how a given
85 participant has integrated previous sequential evidence. Future work could extend this
86 method to more directly interrogate how predictive uncertainty is represented
87 throughout the brain on a moment-by-moment basis.

88   In summary, we found evidence that people could dynamically adapt the spread
89 of spatial attention, and that the retinotopic extent of attentional enhancement of the
90 BOLD response reflected this dynamic adaptation. These findings address a gap in our
91 understanding of spatial attentional control, supporting core theoretical models of
92 attention. Our modeling approach also lays the groundwork to address further questions
93 related to how the attentional field interacts with the non-uniformity of spatial
94 representations and how uncertainty in spatial contexts is represented in the human
95 brain.

References

1) Andersson, J.L.R., Skare, S. and Ashburner, J. (2003) 'How to correct susceptibility distortions in spin-echo echo-planar images: application to diffusion tensor imaging', *NeuroImage*, 20(2), pp. 870–888. Available at: https://doi.org/10.1016/S1053-8119(03)00336-7.

2) Anton-Erxleben, K. and Carrasco, M. (2013) 'Attentional enhancement of spatial resolution: linking behavioural and neurophysiological evidence', *Nature Reviews Neuroscience*, 14(3), pp. 188–200. Available at: https://doi.org/10.1038/nrn3443.

3) Bakst, L. and McGuire, J.T. (2021) 'Eye movements reflect adaptive predictions and predictive precision', *Journal of Experimental Psychology: General*, 150(5), pp. 915–929. Available at: https://doi.org/10.1037/xge0000977.

4) Bakst, L. and McGuire, J.T. (2023) 'Experience-driven recalibration of learning from surprising events', *Cognition*, 232, p. 105343. Available at: https://doi.org/10.1016/j.cognition.2022.105343.

5) Behrens, T.E.J. *et al.* (2007) 'Learning the value of information in an uncertain world', *Nature Neuroscience*, 10(9), pp. 1214–1221. Available at: https://doi.org/10.1038/nn1954.

6) Beilen, M. van *et al.* (2011) 'Attentional Window Set by Expected Relevance of Environmental Signals', *PLOS ONE*, 6(6), p. e21262. Available at: https://doi.org/10.1371/journal.pone.0021262.

7) Benson, N.C. *et al.* (2018) 'The Human Connectome Project 7 Tesla retinotopy dataset: Description and population receptive field analysis', *Journal of Vision*, 18(13), p. 23. Available at: https://doi.org/10.1167/18.13.23.

8) Bloem, I.M. and Ling, S. (2019) 'Normalization governs attentional modulation within human visual cortex', *Nature Communications*, 10(1), p. 5660. Available at: https://doi.org/10.1038/s41467-019-13597-1.

9) Brefczynski, J.A. and DeYoe, E.A. (1999) 'A physiological correlate of the "spotlight" of visual attention', *Nature Neuroscience*, 2(4), pp. 370–374. Available at: https://doi.org/10.1038/7280.

10) Carrasco, M. (2011) 'Visual attention: The past 25 years', *Vision Research*, 51(13), pp. 1484–1525. Available at: https://doi.org/10.1016/j.visres.2011.04.012.

11) Castiello, U. and Umiltà, C. (1990) 'Size of the attentional focus and efficiency of processing', *Acta Psychologica*, 73(3), pp. 195–209. Available at: https://doi.org/10.1016/0001-6918(90)90022-8.

12) D'Acremont, M. and Bossaerts, P. (2016) 'Neural Mechanisms Behind Identification of Leptokurtic Noise and Adaptive Behavioral Response', *Cerebral Cortex*, 26(4), pp. 1818–1830. Available at: https://doi.org/10.1093/cercor/bhw013.

133 13) Datta, R. and DeYoe, E.A. (2009) 'I know where you are secretly attending! The
134   topography of human visual attention revealed with fMRI', *Vision Research*, 49(10),
135   pp. 1037–1044. Available at: https://doi.org/10.1016/j.visres.2009.01.014.

136 14) Daw, N.D. *et al.* (2006) 'Cortical substrates for exploratory decisions in humans',
137   *Nature*, 441(7095), pp. 876–879. Available at: https://doi.org/10.1038/nature04766.

138 15) Dumoulin, S.O. and Wandell, B.A. (2008) 'Population receptive field estimates in
139   human visual cortex', *NeuroImage*, 39(2), pp. 647–660. Available at:
140   https://doi.org/10.1016/j.neuroimage.2007.09.034.

141 16) Eriksen, C.W. and St. James, J.D. (1986) 'Visual attention within and around the field
142   of focal attention: A zoom lens model', *Perception & Psychophysics*, 40(4), pp. 225–
143   240. Available at: https://doi.org/10.3758/BF03211502.

144 17) Favila, S.E., Kuhl, B.A. and Winawer, J. (2022) 'Perception and memory have distinct
145   spatial tuning properties in human visual cortex', *Nature Communications*, 13(1), p.
146   5864. Available at: https://doi.org/10.1038/s41467-022-33161-8.

147 18) Feldmann-Wüstefeld, T. and Awh, E. (2020) 'Alpha-band Activity Tracks the Zoom
148   Lens of Attention', *Journal of Cognitive Neuroscience*, 32(2), pp. 272–282. Available
149   at: https://doi.org/10.1162/jocn_a_01484.

150 19) Fischl, B. (2012) 'FreeSurfer', *NeuroImage*, 62(2), pp. 774–781. Available at:
151   https://doi.org/10.1016/j.neuroimage.2012.01.021.

152 20) Gobell, J.L., Tseng, C. and Sperling, G. (2004) 'The spatial distribution of visual
153   attention', *Vision Research*, 44(12), pp. 1273–1296. Available at:
154   https://doi.org/10.1016/j.visres.2004.01.012.

155 21) Greve, D.N. and Fischl, B. (2009) 'Accurate and robust brain image alignment using
156   boundary-based registration', *NeuroImage*, 48(1), pp. 63–72. Available at:
157   https://doi.org/10.1016/j.neuroimage.2009.06.060.

158 22) Herrmann, K. *et al.* (2010) 'When size matters: attention affects performance by
159   contrast or response gain', *Nature Neuroscience*, 13(12), pp. 1554–1559. Available
160   at: https://doi.org/10.1038/nn.2669.

161 23) Hopf, J.-M. *et al.* (2006) 'The Neural Site of Attention Matches the Spatial Scale of
162   Perception', *Journal of Neuroscience*, 26(13), pp. 3532–3540. Available at:
163   https://doi.org/10.1523/JNEUROSCI.4510-05.2006.

164 24) Huang, D. *et al.* (2017) 'The time course of attention modulation elicited by spatial
165   uncertainty', *Vision Research*, 138, pp. 50–58. Available at:
166   https://doi.org/10.1016/j.visres.2017.06.008.

167 25) Intriligator, J. and Cavanagh, P. (2001) 'The Spatial Resolution of Visual Attention',
168   *Cognitive Psychology*, 43(3), pp. 171–216. Available at:
169   https://doi.org/10.1006/cogp.2001.0755.

170   26) Itthipuripat, S. *et al.* (2014) 'Changing the Spatial Scope of Attention Alters Patterns
171   of Neural Gain in Human Cortex', *Journal of Neuroscience*, 34(1), pp. 112–123.
172   Available at: https://doi.org/10.1523/JNEUROSCI.3943-13.2014.

173   27) Jigo, M., Heeger, D.J. and Carrasco, M. (2021) 'An image-computable model of how
174   endogenous and exogenous attention differentially alter visual perception',
175   *Proceedings of the National Academy of Sciences*, 118(33), p. e2106436118.
176   Available at: https://doi.org/10.1073/pnas.2106436118.

177   28) Kastner, S. *et al.* (1998) 'Mechanisms of Directed Attention in the Human Extrastriate
178   Cortex as Revealed by Functional MRI', *Science*, 282(5386), pp. 108–111. Available
179   at: https://doi.org/10.1126/science.282.5386.108.

180   29) Kay, K.N. *et al.* (2013) 'Compressive spatial summation in human visual cortex',
181   *Journal of Neurophysiology*, 110(2), pp. 481–494. Available at:
182   https://doi.org/10.1152/jn.00105.2013.

183   30) Kınıklıoğlu, M. and Boyaci, H. (2022) 'Increasing the spatial extent of attention
184   strengthens surround suppression', *Vision Research*, 199, p. 108074. Available at:
185   https://doi.org/10.1016/j.visres.2022.108074.

186   31) Klein, B.P., Harvey, B.M. and Dumoulin, S.O. (2014) 'Attraction of Position Preference
187   by Spatial Attention throughout Human Visual Cortex', *Neuron*, 84(1), pp. 227–237.
188   Available at: https://doi.org/10.1016/j.neuron.2014.08.047.

189   32) Maunsell, J.H.R. (2015) 'Neuronal Mechanisms of Visual Attention', *Annual Review of
190   Vision Science*, 1(Volume 1, 2015), pp. 373–391. Available at:
191   https://doi.org/10.1146/annurev-vision-082114-035431.

192   33) McAdams, C.J. and Maunsell, J.H. (1999) 'Effects of attention on orientation-tuning
193   functions of single neurons in macaque cortical area V4', *The Journal of
194   Neuroscience: The Official Journal of the Society for Neuroscience*, 19(1), pp. 431–
195   441. Available at: https://doi.org/10.1523/JNEUROSCI.19-01-00431.1999.

196   34) McGuire, J.T. *et al.* (2014) 'Functionally Dissociable Influences on Learning Rate in a
197   Dynamic Environment', *Neuron*, 84(4), pp. 870–881. Available at:
198   https://doi.org/10.1016/j.neuron.2014.10.013.

199   35) McMains, S.A. and Somers, D.C. (2004) 'Multiple Spotlights of Attentional Selection
200   in Human Visual Cortex', *Neuron*, 42(4), pp. 677–686. Available at:
201   https://doi.org/10.1016/S0896-6273(04)00263-6.

202   36) Moeller, S. *et al.* (2010) 'Multiband multislice GE-EPI at 7 tesla, with 16-fold
203   acceleration using partial parallel imaging with application to high spatial and
204   temporal whole-brain fMRI', *Magnetic Resonance in Medicine*, 63(5), pp. 1144–1153.
205   Available at: https://doi.org/10.1002/mrm.22361.

206   37) Müller, N.G. *et al.* (2003) 'A Physiological Correlate of the "Zoom Lens" of Visual
207   Attention', *Journal of Neuroscience*, 23(9), pp. 3561–3565. Available at:
208   https://doi.org/10.1523/JNEUROSCI.23-09-03561.2003.

209 38) Nadarajah, S. (2005) 'A generalized normal distribution', *Journal of Applied Statistics*,
210   32(7), pp. 685–694. Available at: https://doi.org/10.1080/02664760500079464.

211 39) Nassar, M.R. *et al.* (2010) 'An Approximately Bayesian Delta-Rule Model Explains the
212   Dynamics of Belief Updating in a Changing Environment', *Journal of Neuroscience*,
213   30(37), pp. 12366–12378. Available at: https://doi.org/10.1523/JNEUROSCI.0822-
214   10.2010.

215 40) Nassar, M.R. *et al.* (2012) 'Rational regulation of learning dynamics by pupil-linked
216   arousal systems', *Nature Neuroscience*, 15(7), pp. 1040–1046. Available at:
217   https://doi.org/10.1038/nn.3130.

218 41) Nassar, M.R., Bruckner, R. and Frank, M.J. (2019) 'Statistical context dictates the
219   relationship between feedback-related EEG signals and learning', *eLife*. Edited by
220   T.H. Donner et al., 8, p. e46975. Available at: https://doi.org/10.7554/eLife.46975.

221 42) O'Reilly, J.X. *et al.* (2013) 'Dissociable effects of surprise and model update in parietal
222   and anterior cingulate cortex', *Proceedings of the National Academy of Sciences*,
223   110(38), pp. E3660–E3669. Available at: https://doi.org/10.1073/pnas.1305373110.

224 43) Palmer, J. and Moore, C.M. (2009) 'Using a filtering task to measure the spatial extent
225   of selective attention', *Vision Research*, 49(10), pp. 1045–1064. Available at:
226   https://doi.org/10.1016/j.visres.2008.02.022.

227 44) Payzan-LeNestour, E. *et al.* (2013) 'The Neural Representation of Unexpected
228   Uncertainty during Value-Based Decision Making', *Neuron*, 79(1), pp. 191–201.
229   Available at: https://doi.org/10.1016/j.neuron.2013.04.037.

230 45) Payzan-LeNestour, E. and Bossaerts, P. (2011) 'Risk, Unexpected Uncertainty, and
231   Estimation Uncertainty: Bayesian Learning in Unstable Settings', *PLOS*
232   *Computational Biology*, 7(1), p. e1001048. Available at:
233   https://doi.org/10.1371/journal.pcbi.1001048.

234 46) Posner, M.I. (1980) 'Orienting of Attention', *Quarterly Journal of Experimental*
235   *Psychology*, 32(1), pp. 3–25. Available at:
236   https://doi.org/10.1080/00335558008248231.

237 47) Preuschoff, K., 't Hart, B.M. and Einhauser, W. (2011) 'Pupil Dilation Signals Surprise:
238   Evidence for Noradrenaline's Role in Decision Making', *Frontiers in Neuroscience*, 5.
239   Available at: https://doi.org/10.3389/fnins.2011.00115.

240 48) Puckett, A.M. and DeYoe, E.A. (2015) 'The Attentional Field Revealed by Single-Voxel
241   Modeling of fMRI Time Courses', *Journal of Neuroscience*, 35(12), pp. 5030–5042.
242   Available at: https://doi.org/10.1523/JNEUROSCI.3754-14.2015.

243 49) Reuter, M., Rosas, H.D. and Fischl, B. (2010) 'Highly accurate inverse consistent
244   registration: A robust approach', *NeuroImage*, 53(4), pp. 1181–1196. Available at:
245   https://doi.org/10.1016/j.neuroimage.2010.07.020.

246 50) Reynolds, J.H. and Heeger, D.J. (2009) 'The Normalization Model of Attention',
247   *Neuron*, 61(2), pp. 168–185. Available at:
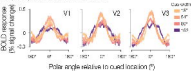248   https://doi.org/10.1016/j.neuron.2009.01.002.

249 51) Samaha, J., Sprague, T.C. and Postle, B.R. (2016) 'Decoding and Reconstructing the
250   Focus of Spatial Attention from the Topography of Alpha-band Oscillations', *Journal*
251   *of cognitive neuroscience*, 28(8), pp. 1090–1097. Available at:
252   https://doi.org/10.1162/jocn_a_00955.

253 52) Setsompop, K. *et al.* (2012) 'Blipped-controlled aliasing in parallel imaging for
254   simultaneous multislice echo planar imaging with reduced g-factor penalty',
255   *Magnetic Resonance in Medicine*, 67(5), pp. 1210–1224. Available at:
256   https://doi.org/10.1002/mrm.23097.

257 53) Shaw, M.L. and Shaw, P. (1977) 'Optimal allocation of cognitive resources to spatial
258   locations', *Journal of Experimental Psychology: Human Perception and Performance*,
259   3(2), pp. 201–211. Available at: https://doi.org/10.1037/0096-1523.3.2.201.

260 54) Shioiri, S. *et al.* (2016) 'Visual attention spreads broadly but selects information
261   locally', *Scientific Reports*, 6(1), p. 35513. Available at:
262   https://doi.org/10.1038/srep35513.

263 55) Smith, S.M. *et al.* (2004) 'Advances in functional and structural MR image analysis
264   and implementation as FSL', *NeuroImage*, 23, pp. S208–S219. Available at:
265   https://doi.org/10.1016/j.neuroimage.2004.07.051.

266 56) Sprague, T.C. and Serences, J.T. (2013) 'Attention modulates spatial priority maps in
267   the human occipital, parietal and frontal cortices', *Nature Neuroscience*, 16(12), pp.
268   1879–1887. Available at: https://doi.org/10.1038/nn.3574.

269 57) Taylor, J.E.T. *et al.* (2015) 'Attentional cartography: mapping the distribution of
270   attention across time and space', *Attention, Perception, & Psychophysics*, 77(7), pp.
271   2240–2246. Available at: https://doi.org/10.3758/s13414-015-0943-0.

272 58) Tkacz-Domb, S. and Yeshurun, Y. (2018) 'The size of the attentional window when
273   measured by the pupillary response to light', *Scientific Reports*, 8(1), p. 11878.
274   Available at: https://doi.org/10.1038/s41598-018-30343-7.

275 59) Tünçok, E., Carrasco, M. and Winawer, J. (2024) 'Spatial attention alters visual
276   cortical representation during target anticipation'. bioRxiv, p. 2024.03.02.583127.
277   Available at: https://doi.org/10.1101/2024.03.02.583127.

278 60) Vo, V.A., Sprague, T.C. and Serences, J.T. (2017) 'Spatial Tuning Shifts Increase the
279   Discriminability and Fidelity of Population Codes in Visual Cortex', *Journal of*
280   *Neuroscience*, 37(12), pp. 3386–3401. Available at:
281   https://doi.org/10.1523/JNEUROSCI.3484-16.2017.

282 61) Yeshurun, Y. (2019) 'The spatial distribution of attention', *Current Opinion in*
283   *Psychology*, 29, pp. 76–81. Available at:
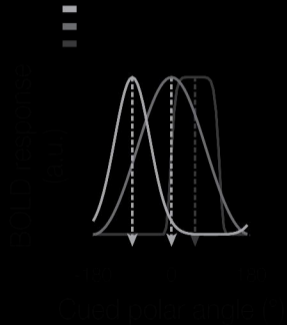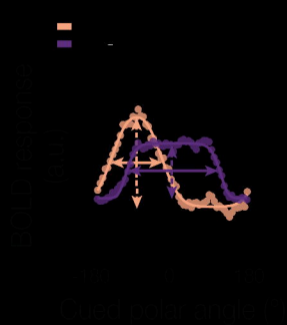284   https://doi.org/10.1016/j.copsyc.2018.12.008.

285
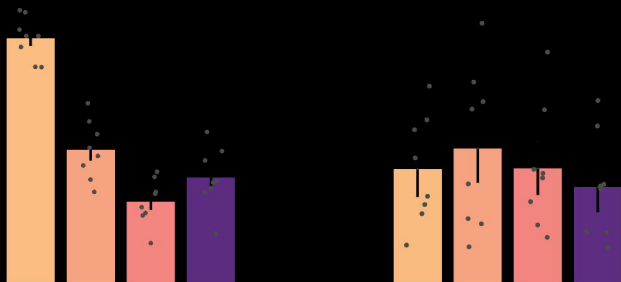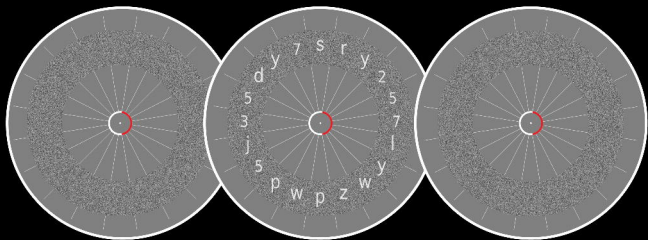
a. Annular V1 BOLD activity reconstruction
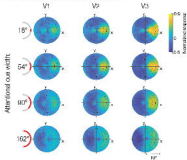
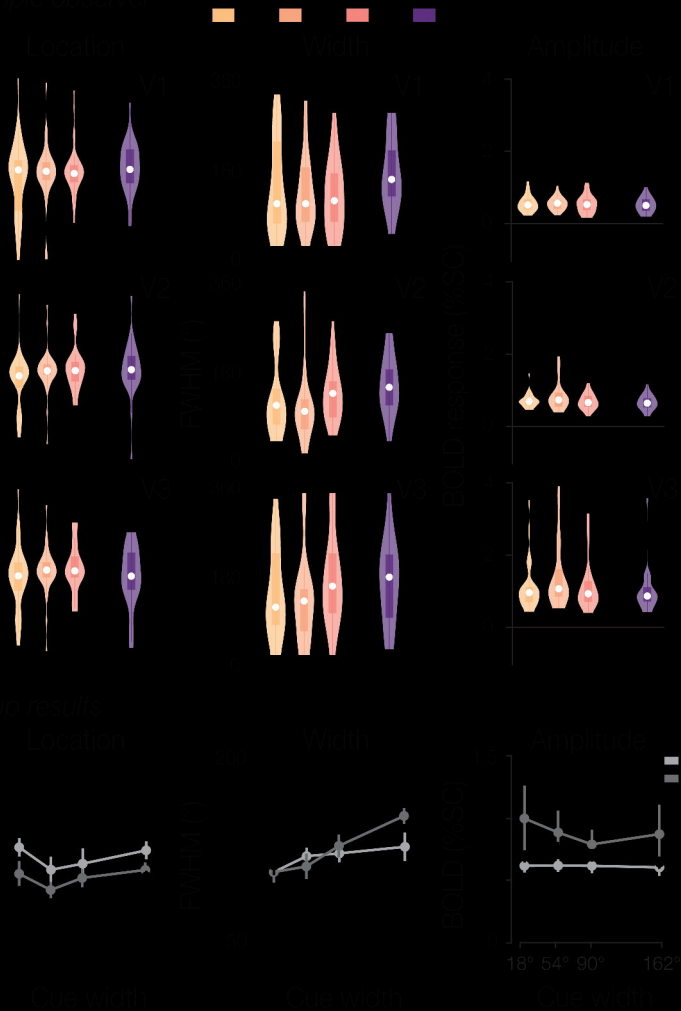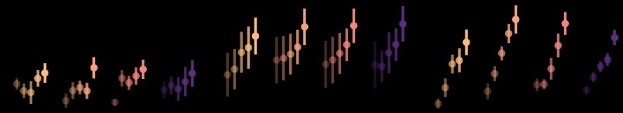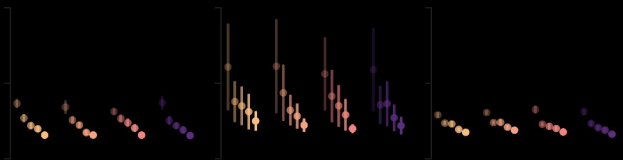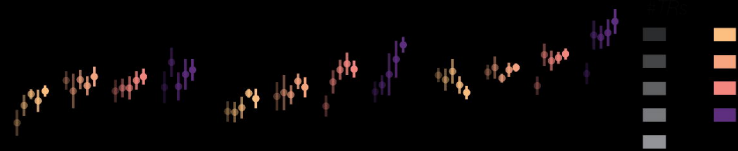**b.** Spatial profile attentional modulation

Pollar angle relative to cued location (°)
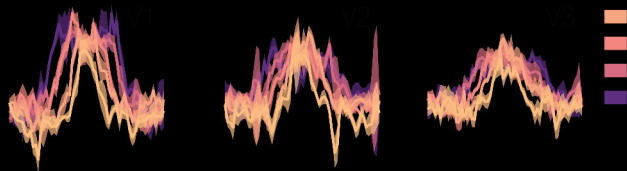
a. *Generalized Gaussian model*

b. *Quantify attentional field*

BOLD response (a.u.)

Cued polar angle (°)

BOLD response (a.u.)

Cued polar angle (°)

a. *Example observer*

Location — Width — Amplitude

V1, V2, V3 panels

Angular error (°) — FWHM (°) — BOLD response (±SD)

b. *Group results*

Location — Width — Amplitude

|angular error| (°) — FWHM (°) — BOLD (±SD)

18° 54° 90° 162°

Cue width — Cue width — Cue width

a. Spatial profile contrast modulation

BOLD response
(% signal change)

V1   V2   V3

Polar angle relative to center location (°)

b. Group results

Location   Width   Amplitude

Angular error (°)   FWHM (°)   BOLD (%SD)

Contrast width   Contrast width   Contrast width

18° 54° 90°126°162°

c. FWHM comparison

FWHM
Contrast modulation (°)

FWHM
Attention field (°)